J Mater Sci: Mater Electron (2016) 27:9476–9482
DOI 10.1007/s10854-016-4996-1

In-situ sol–gel synthesis of luminescent Mn^{2+}-doped zinc silicate nanophosphor

K. Omri[1] · L. El Mir[1,2]

Received: 23 March 2016 / Accepted: 14 May 2016 / Published online: 24 May 2016

Abstract Nanocrystalline undoped and Mn^{2+}-doped zinc silicate (α-Zn_2SiO_4:Mn) nanophosphors were in situ prepared by a sol–gel technique. The crystallite morphology for Mn-doped and undoped nanophosphors have been determined by X-ray diffraction and transmission electron microscopy. In the case of undoped Zn_2SiO_4 nanophosphors, the powder with an average particle size around 80 nm shows a strong luminescence band centred at 760 nm at room temperature in the visible range. In addition, Zn_2SiO_4:Mn nanophosphors emit very strong green luminescence (525 nm), which originated from the $^4T_1$–$^6A_1$ transitions of Mn^{2+} ions. The luminescence spectra and lifetime of the excited state of Mn^{2+} ions-doped Zn_2SiO_4 nanocrystals are investigated.

1 Introduction

Inorganic phosphors are some of the most fundamental materials that support modern society with their wide application in lighting devices, displays, and information for humankind [1]. At present, the commercialized phosphor YBO_3 is commonly used as the green phosphor for plasma display panels (PDP) [2]. Therefore, this phosphor has a relatively long decay time, which will influence its use for PDP [2, 3]. So, searching green phosphors with improved qualities, for example, with short decay time, is necessary to improve the luminance properties of PDP [3]. Also, compared to the present commercial YBO_3 green phosphors, the Mn^{2+} activated Zn_2SiO_4 phosphor may accommodate advantages such as better thermal stability, less outgassing, chemically inert to plasmas commonly used in plasma operated panels and do not contaminate the electron emitters in field emission displays and so on [4, 5].

Therefore, among the many inorganic phosphors, α-Zn_2SiO_4:Mn^{2+} has been widely used in industry as a green-emitting phosphor for plasma display panels due to its high luminescence efficiency and its highly physical and chemical stability [6]. Zn_2SiO_4 has been identified as a promising host matrix for many rare earths and transition metal dopant ions [7]. It possesses a rhombohedral structure (space group), wide energy band gap (5.5 eV), excellent chemical stability and also presents the advantage of highly saturated color [8], which makes it a promising nano-material for the various industrial applications. Manganese activated zinc orthosilicate is one of the earliest known phosphors [9]. As the Mn^{2+} ion is substituted into the Zn^{2+} sites in the Zn_2SiO_4 host crystal, it acts as a luminescence center, giving green-emission for α-Zn_2SiO_4 phase [10] or yellow-emission for β-Zn_2SiO_4 phase [11]. It is understood that the d–d transition from the $^4T_1(^4G)$ excited-state to the $^6A_1(^6S)$ ground-state in the 3d outermost orbital of the Mn^{2+} ion generates a green- or yellow-emission depending on the strength of its surrounding crystal field [11]. For this research, the zinc silicate family is a highly versatile material as evident from the properties of α-Zn_2SiO_4, which has the possibility of being a multi-color phosphor by inserting various guest ions instead of Mn^{2+} ions, such as Ga^{3+} for violet-emission [12], Ce^{3+}

✉ K. Omri
omrikarim16@yahoo.fr

[1] Laboratoire de Physique des Matériaux et des Nanomatériaux Appliquée à l'Environnement, Faculté des Sciences de Gabès, Cité Erriadh Manara Zrig, 6072 Gabès, Tunisia

[2] Departement of Physics, College of Sciences, Al Imam Mohammad Ibn Saud Islamic University (IMSIU), Riyadh 11623, Saudi Arabia

[13] or Eu^{2+} [14] for blue-emission, and Eu^{3+} [15] for red-emission as discussed in depth in a review [3].

Numerous studies had focused on developing chemical reaction methods to prepare highly efficient Zn_2SiO_4:Mn^{2+} phosphors. Taghavinia et al. used porous silicon as one of the starting materials and impregnated porous silicon layers with luminescent Zn_2SiO_4:Mn^{2+} particles [16]. Porous silicon was directly involved in the reaction responsible for the formation of luminescent Zn_2SiO_4:Mn^{2+} phosphors. The phosphor particles were obtained inside a transparent porous body, making it possible to activate porous silicon layers with highly efficient phosphors [16–18].

In this study, the method is applied to prepare Zn_2SiO_4 and 5 at.% Mn doped Zn_2SiO_4 particles embedded in silica monolith by the same protocol of sol–gel method, Mn doped zinc oxide nanoparticles and studied the structural and optical properties of the obtained nanophosphors. The emissions, thus observed are discussed using a schematic energy level diagram.

2 Experimental

2.1 Synthesis

In the present investigation Mn doped and undoped Zn_2SiO_4 nanophosphors were synthesized by a sol–gel method. The nano-crystalline 5 at.% Mn doped and undoped ZnO aerogels were prepared by a sol–gel method under super-critical conditions of ethyl alcohol (EtOH) based on K. Omri et al. protocol [19]. 5 at.% Mn doped and undoped Zn_2SiO_4 nanophosphors samples were prepared by sol–gel method according to El Mir protocol [11, 19]

2.2 Characterizations

In order to confirm the phase and determine the crystal parameters, the Mn doped and undoped Zn_2SiO_4 nanophosphors samples in two cases were characterized by X-ray diffraction (XRD) using a Bruker D5005 powder. Transmission electron microscopy (TEM, JEM-200CX) was used to study the morphology and particle size of the nano-phosphor powders. For photoluminescence (PL) measurements, the 450-W Xenon lamp was used as an excitation source. The emitted light from the sample collected by an optical fiber on the same side as that of excitation was analyzed with a Jobin-Yvon Spectrometer HR460 and a multichannel CCD detector (2000 pixels). The photoluminescence excitation (PLE) measurements were performed on a Jobin-Yvon Fluorolog 3-2 spectrometer. The low temperature experiments were carried out in a Janis VPF-600 Dewar with variable temperature controlled between 78 and 300 K.

3 Results and discussion

3.1 Structural studies

The X-ray diffraction patterns of Zn_2SiO_4 (a), Zn_2SiO_4:Mn (b) nanophosphors and Mn doped ZnO nanoparticles (inset) have been presented in Fig. 1. In the case of ZnO:Mn nanoparticles, we noticed the appearance of pronounced diffraction peaks, which can be attributed to the planes of ZnO, respectively [7]. The obtained XRD spectra matched well with the space group $P6_3mc$ (186) (No. 36–1451) of wurtzite ZnO structure [7, 19]. The lattice constants calculated from the XRD pattern, which are very close to ZnO ones, i.e., $a = 3.2498$ Å and $c = 5.2066$ Å [20–22]. The average crystallite size (D) was estimated from the line broadening in X-ray powder using Scherrer's equation [23].

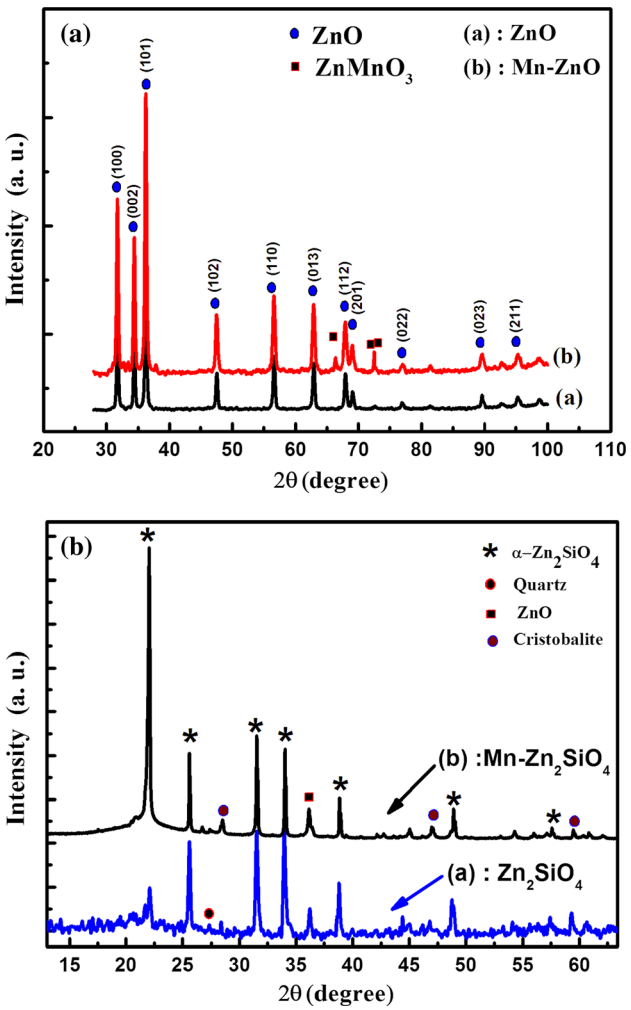

Fig. 1 X-ray diffraction pattern of the **a** undoped and Mn doped ZnO nanopowder and **b** undoped and Mn doped Zn_2SiO_4 nanophosphors

$$D = \frac{0.9\lambda}{B\cos\theta_B} \quad (1)$$

where λ is the X-ray wavelength (λ = 1.5418 Å), θ_B is the maximum of the Bragg diffraction peak (rad) and B is the line width at half maximum.

After a correction for the instrumental broadening, an average size value of the crystallites was found to be 24 nm. In the case of our nanophosphors, a new zincic (α-Zn_2SiO_4) compound was formed. The analysis of XRD data of Zn_2SiO_4 phases is usually qualitative, just based on relative peak intensities. Therefore, the hexagonal ZnO and willemite Zn_2SiO_4 may coexist in the composite [7]. The willemite (α-Zn_2SiO_4) crystals were well developed. This analysis shows that the peaks these samples are indexed to the α-Zn_2SiO_4 according to the registers in the International Centre for Diffraction Data (ICDD) data base (JCPDS Card 37–1485) [6, 7]. The difference in the peak intensity and width shows that the seeded sample has a higher degree of crystallinity. The lattice constants calculated from the XRD pattern are $a = 13.944$ Å and $c = 9.314$ Å, which are very close to willemite α-Zn_2SiO_4 ones, i.e., [6]. This result indicates that α-Zn_2SiO_4 has a rhombohedral structure [6]. It is to be noted that the small amount of doped ions Mn^{2+} have almost no effect on the basic crystal structure of Zn_2SiO_4. Therefore, this is indicative of the entire dissolution of Mn^{2+} into the host lattice. It has also been observed in the case of Mn^{2+} doped Zn_2SiO_4, a low angle shift in XRD patterns, resulting in the lattice parameters of Zn_2SiO_4 increase. This result strongly indicated the Mn substitution for Zn, is mainly attributed to the substitution of larger sized Mn^{2+} (0.66 Å) for smaller Zn^{2+} (0.60 Å) ions.

The average grain size of the crystallites Zn_2SiO_4:Mn varies from 70 to 90 nm [7], has been estimated using Scherrer's formula (1). However, XRD gives no information on the actual distribution of crystallite sizes in the particles.

To confirm the results obtained by XRD and to learn more about the morphology of our samples, we performed an analysis by transmission electron microscopy (TEM). Figure 2 shows the TEM micrographs of our nanophosphors indicating that the well-crystallized Zn_2SiO_4 particles. At high temperature at 1200 °C, Zn and Si species, move and diffuse inside the porous body to form Zn_2SiO_4 phase with a particle size greater than 80 nm. The particles were observed to be irregular shaped, highly dispersed and the average size was found to be in the range 60–80 nm. The disadvantage of this technique is the low counting statistics and high time consumption due to the requirement of having to analyze a large number of grains. The composition of the powder nanophosphors has been measured using EDX. Energy dispersive X-ray spectroscopy (EDX) is a standard procedure for identifying and quantifying

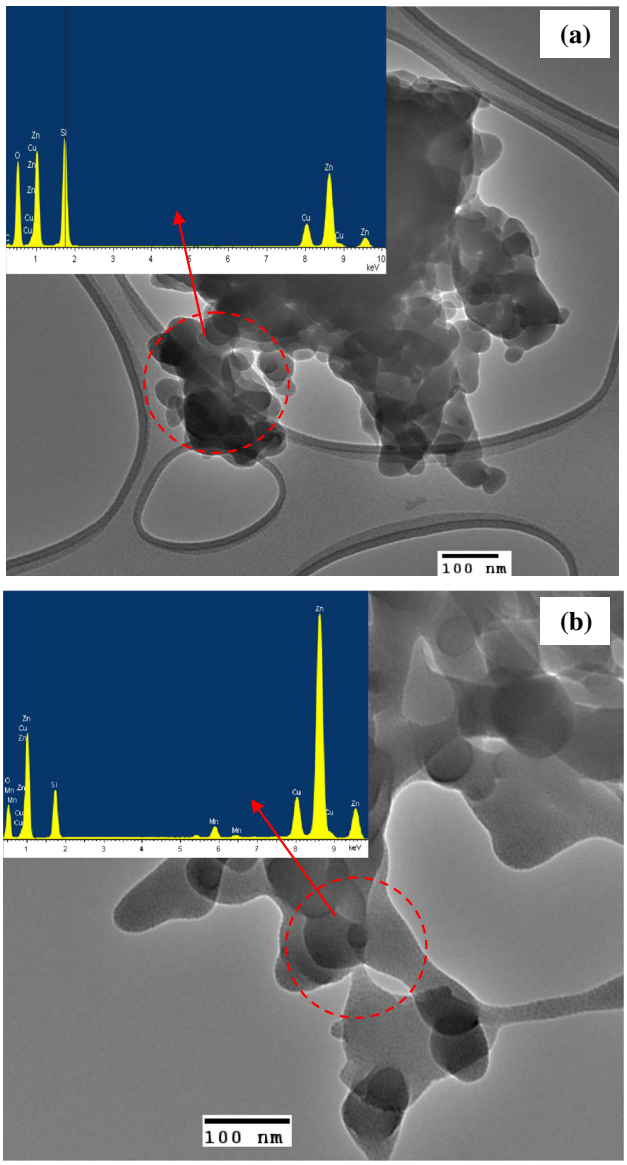

Fig. 2 Typical TEM photograph showing the general morphology **a** undoped Zn_2SiO_4 and **b** Zn_2SiO_4:Mn nanophosphors and its EDX analysis

elemental composition of sample area as small as a few nanometers. Energy dispersive spectroscopy (EDX) analysis during the TEM observation, shown in Fig. 2, confirms the XRD results. The existence of manganese (Mn) in the prepared sample is clear in the EDX spectra. There appeared no other emissions apart from Si, Zn, Mn, and O in EDX spectra of the sample. This result confirm the formation of Zn_2SiO_4:Mn nanophosphors.

3.2 Photoluminescence property

To further characterize the optical responses of our samples, we present in the following, the different properties of

luminescence nanoparticles in a silica matrix. In the present investigation, the emission and excitation spectra of Zn_2SiO_4 nanophosphors are shown in Fig. 3. The spectrum shows two broadband emissions, the first one centered at 760 nm and the second in the range 375 nm. Nevertheless, the striking feature is the absence of almost any of the usually reported visible emission bands in the range 400–650 nm (2.4–2.7 eV), and the appearance of a strong and wide near infrared (NIR) emission band centered around 760 nm, besides a near band edge emission including the bound exciton line. The observed UV–visible emission band is also quite different from what is usually seen [7]. On the other hand, the PLE spectrum detected at 760 nm which shows the appearance of a very weak peak at 375 nm (3.3 eV) relative to its value at higher energy (inset of Fig. 3). The low energy excitation band is due to carrier excitation in the near band edge of ZnO nanoparticles [7]. Indeed, as it has been shown by Chakrabarti et al. [24], a high annealing temperature (1073 K) results in a rapid grain growth and when the radii of the nanoparticles increases to 8.2 nm, a bulk ZnO like band gap is obtained. However, the most efficient excitation process is with photon energies of about 5.4 eV (230 nm), which are much higher than the ZnO bulk band gap. Unfortunately, the high energy peak position of the PLE spectrum cannot be clearly determined due to the high energy range limit of our setup. The shape and the structured nature of the PL emission band, the large shift between the PL and the PLE energy peaks of the 760 nm PL emission are in principle a signature of a deep level emission with an electron–phonon coupling. However, its full width at half maximum (FWHM) dependence with temperature cannot be fitted according to this model, which rules out the hypothesis of an electron–phonon coupling [7]. We suggest that this luminescence band (760 nm) is attributed to the contribution in the formation of a non-bridging oxygen hole (NBOHs) excited at the spectral region $h\nu \geq 5.4$ eV, such band arises from the absorption of Zn_2SiO_4 particles [7].

Upon incorporation of the ZnO:Mn in the silica matrix and thermal treatment at 1200 °C, PL spectra illustrated in Fig. 4 show the appearance of a strong luminescence band centered at 525 nm. However, the synthesis and luminescence properties of our nanometer-sized nanophosphor material are rarely reported. Excellent luminescence properties of Zn_2SiO_4:Mn nanophosphor comparing with other reference paper. The green emission has been assigned to an electronic transition of $^4T_1(^4G) \rightarrow {}^6A_1(^6S)$ peaking at the wavelength 525 nm and which is a parity forbidden emission transition of Mn^{2+} ions [25]. With 255 nm excitation wavelength, we also note the change of the PL intensity with temperature, which is an increase of PL intensity when the measurement temperature decreases. This is due to d–d transition on Mn^{2+} as the relevant luminescent center. This emission centered at 525 nm, corresponds to the energy transfer in the Mn ions [26]. With Mn^{2+} occupies part of the Zn^{2+} site, which is coordinated by four oxygen atoms [25]. The weak crystal field around Mn^{2+} results in the low splitting width of its 3d energy levels, in accordance with the observations of Stevels et al. [27]. As a result, an emission at high energy (green) is observed. The red-shift of the emission band with the increasing temperature is due to the exchange interactions between ions with the Mn^{2+} ions (Fig. 5) [28]. In willemite the Mn^{2+} ions are situated at the slightly distorted tetrahedral sites with four oxygen neighbors [28]. The applied excitation photon energy of 4.86 eV (255 nm) is smaller than the band gap of Zn_2SiO_4. The excitation of Mn^{2+} ions follows their ionization (transition from the

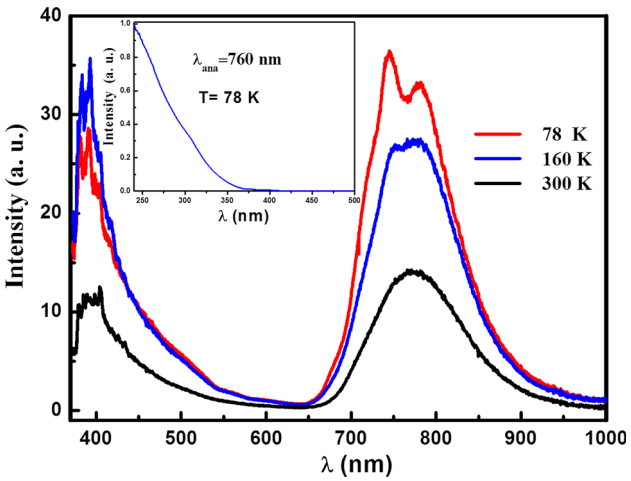

Fig. 3 PL spectrum of a typical Zn_2SiO_4 nanophosphors. The *inset* shows the PLE spectrum of Zn_2SiO_4 nanophosphors

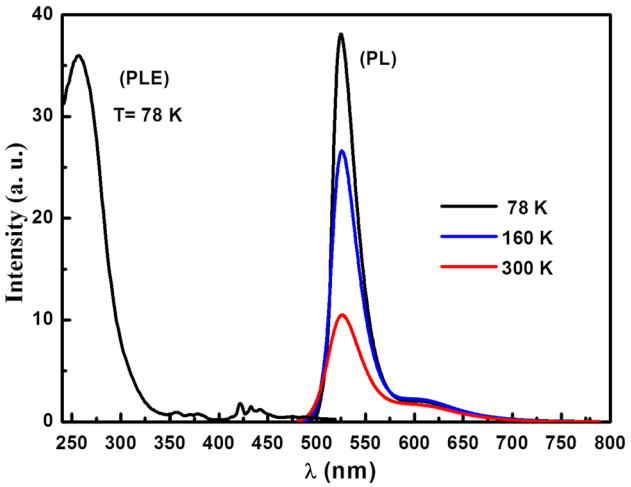

Fig. 4 PL and PLE spectrum of a typical Zn_2SiO_4:Mn nanophosphors

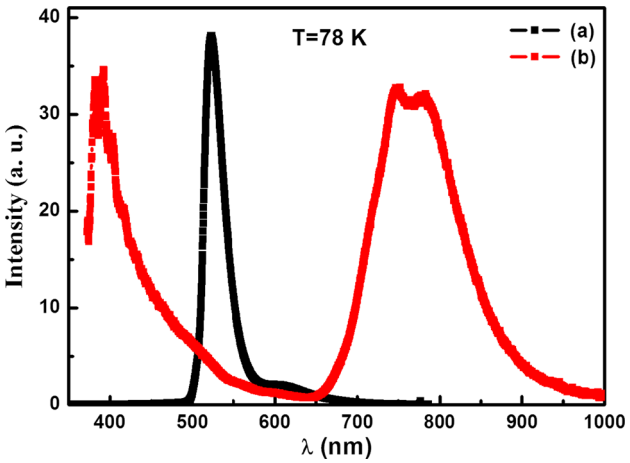

Fig. 5 PL spectrum of a typical Zn_2SiO_4 and Zn_2SiO_4:Mn nanophosphors at 78 K

ground state to the conduction band) and the non-radiative relaxation of the electrons to the excited state $^4T_1$ of Mn^{2+} [29]. From the emission spectra, a slight red-shift of the peak maximum is observed while the emission intensity increases. It is generally recognized that the luminescence of the Mn^{2+} ion depends on the Zn_2SiO_4 host crystal field. Mn^{2+} ions in the Zn_2SiO_4 host with higher crystallinity feel a stronger crystal field. Increasing the crystal field reduces the energy difference of the ground and first excited state, resulting in peak broadening and red-shift of the emission peak [3].

Furthermore, the PLE spectra of the band detected at 525 nm (Fig. 4) show a strong excitation band ranging from 240 to 300 nm with a maximum at about 255 nm (4.9 eV) compared to bands in the UV–Vis range. The band at 255 nm is considered to be responsible for the emission at 525 nm. Furthermore, the spectra fully agree with previously measured excitation spectrum of Zn_2SiO_4:Mn [30]. The broad excitation peak at 255 nm could be attributed to a charge transfer transition (or the ionization of manganese) from the divalent manganese ground state (Mn^{2+}) to the conduction band (CB). This transition will be further discussed later based on the previous literature reports [30, 31]. In addition to the CT band, other bands (inset) of Mn^{2+} (d–d) transitions are also observed at higher wavelengths (350–500 nm), these are caused by crystal field splitting of the 4D and 4G levels as shown by the Orgel diagram for Mn^{2+} [32, 33]. The electrons in the $^6A_1$ (^6S) ground state of Mn^{2+} ions, are excited to the conduction band of Zn_2SiO_4 by photons, and the free electrons in the conduction band relax back to the $^4T_1$ (^4G) excited state through a non-radiative process [34]. Finally, this is followed by a radiative transition from the $^4T_1$ (^4G) excited state to the $^6A_1$ (^6S) ground state, giving rise to a green emission band (525 nm). The mechanism involved in the generation of a green emission from Zn_2SiO_4:Mn^{2+} nanophosphors has been reported earlier and shown schematically in Fig. 6 [25].

We have studied the intensity and the peak energy dependence of the PL band versus the power excitation density of our nanophosphors as can be seen in Figs. 7 and 8. In the case of undoped Zn_2SiO_4 nanophosphors (Fig. 7), the emission intensity (760 nm) shows a linear variation with the power excitation (inset of Fig. 7). Furthermore, no change in the PL spectra, neither the shape nor position, was observed with power excitation, even after being aged for over 90 days, indicating the time stability of the nanophosphors material. This result strongly suggests that the production of nanoparticles in SiO_2 matrix by sol–gel is a simple way to maintain the luminescence spectra of the nanoparticles.

On the other hand, in the case of Mn-doped Zn_2SiO_4 nanophosphors (Fig. 8), it is clear this analysis shows the more significant red-shift and broadening of the UV photoluminescence peak with increasing excitation power. Therefore, the emission intensity (525 nm) shows a similar linear variation with the power excitation which suggest that the two emission bands have the same origin. The green luminescence is the conventional green of α-Zn_2SiO_4:Mn^{2+} nanophosphors, occurring at about 525 nm, a well known, it corresponds to an internal transition of Mn^{2+} in α-Zn_2SiO_4 phase and the second bands in the range 560–608 nm for Mn^{2+} in the β-Zn_2SiO_4 phase [3]. Also, the strong emission peaks around 525 and 590 nm are observed only under the highest excitation power density 70 MW/cm^2 (Fig. 8). The sharpness of the peak can be ascribed as due to the uniformity of particle sizes. The emission intensity shows a linear variation with the power excitation (inset Fig. 8). Furthermore, no change in the PL spectra, neither the shape nor position, was

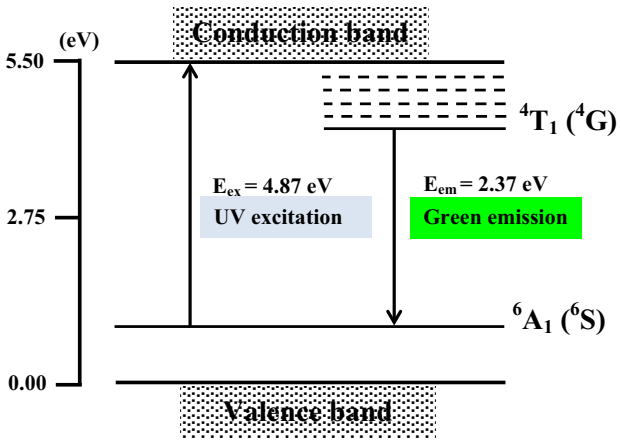

Fig. 6 Energy level scheme describing the *green* color emission process in Zn_2SiO_4:Mn nanophosphors upon excitation with 255 nm (Color figure online)

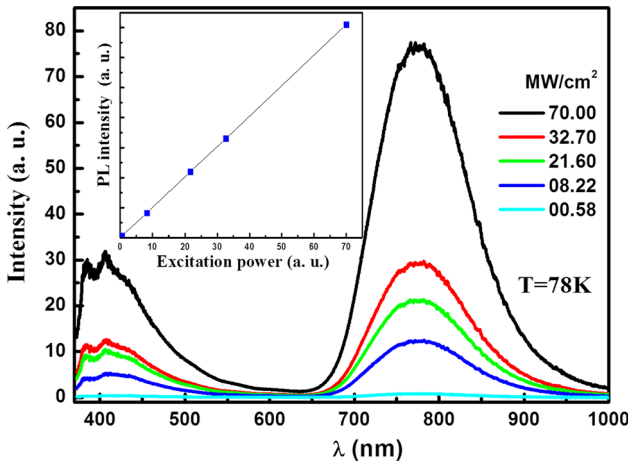

Fig. 7 The variation of the PL intensity with the power excitation density at the UV range of Zn_2SiO_4 nanophosphors

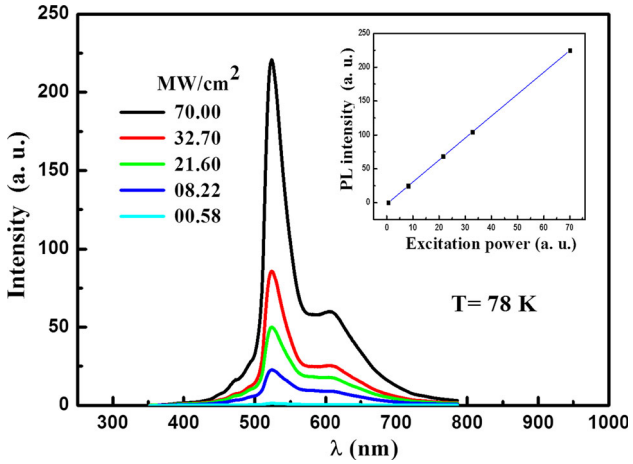

Fig. 8 The variation of the PL intensity with the power excitation density at the UV range of Zn_2SiO_4:Mn nanophosphors

observed with power excitation, even after being aged for a longue period of time, indicating the time stability of the composite material. These results prove that there a origin of the luminescent centre and the nature of this band has so far not completely been established and calls for further investigations, particularly the study of the power excitation effect above 70 MW/cm^2.

However, it is not clearly understood the mechanism of defect emission of composite phosphor under 255 nm excitation. Future work will be focused to understand this mechanism.

The decay curve of the green emission of the α-Zn_2SiO_4:Mn^{2+} nanophosphor is shown in Fig. 9. The decay curve corresponding to the emission band at 525 nm shows that the decay kinetics is a double-exponential decay curve. The result of decay curve can be obtained according to the following equation [33]:

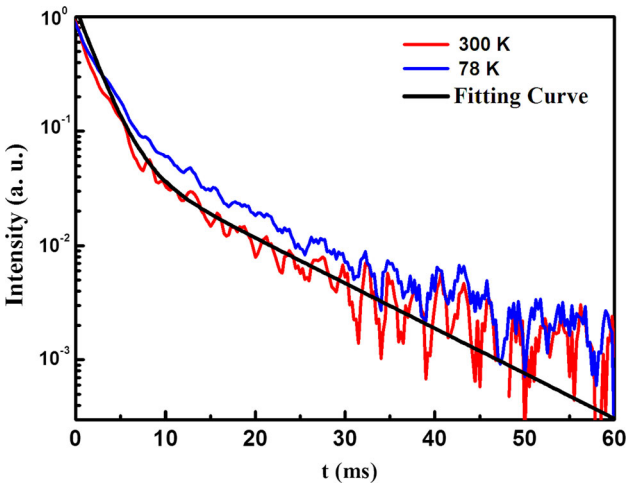

Fig. 9 Decay curve of the Zn_2SiO_4:Mn nanophosphors

$$I = A_f e^{(-t/\tau_f)} + A_s e^{(-t/\tau_s)} \quad (2)$$

where τ_f and τ_s are the fast and slow components of the luminescent lifetimes, A_f and A_s are the weight factors of the two components, respectively. The fitting results are $A_f/A_s = 14.28$, $\tau_f = 2$ ms, $\tau_s = 11$ ms. This is in agreement with the previous observations [33]. The long decay time of Zn_2SiO_4:Mn is an obstacle for the PDP application. Thus, a lot of efforts have been dedicated to shorten the decay time of Zn_2SiO_4:Mn particles without losing the much efficiency [6, 32]. In general, it is possible to reduce the decay time of a phosphor by increasing the manganese dopant content. However, because of the accompanying energy transfer, nonradiative de-excitation processes will increase and the nanophosphors efficiency will decrease due to the well-known dopant concentration effect. When the dopant content is increased, the competition between a higher number of excited centers and lower radiative efficiency will determine the optimal dopant concentration [32]. This information might therefore facilitate a better understanding of the photo-luminescence properties which could possibly be influenced by the crystallite size, which in turn will be a function of the synthesis parameters of nanophosphor materials.

4 Conclusion

In summary, we have synthesized pure and Mn-doped Zn_2SiO_4 nanophosphor using a sol–gel method. The X-ray diffraction and TEM show a crystalline phase with a particle size ranging between 60 and 90 nm. Based on the PL and PLE analysis of undoped Zn_2SiO_4, it can be concluded that the excitation peak near 760 nm can be connected with the formation of NBOHs, such band arises from the

absorption of Zn_2SiO_4 particles. Resulting particles are crystalline, as evidenced by the TEM images and XRD, and they emit green light, indicating the presence of Mn^{2+} in the Mn-doped Zn_2SiO_4 particles. From the analysis of the spectra of PL and PLE, we can be concluded that the green emission (525 nm) has been assigned to an electronic transition of $^4T_1(^4G) \rightarrow {}^6A_1(^6S)$. The advantages of this method include simplified procedure, low annealing temperature, time-saving, controllable size and morphology, large-scale production and wide practicality for other phosphor materials, which have potential applications in displaying and lighting fields.

References

1. C. Feldmann, T. Jüstel, C.R. Ronda, P.J. Schmidt, Adv. Funct. Mater. **13**, 511 (2003)
2. D. Chen, Y. Zhou, W. Xu, J. Zhong, Z. Ji, W. Xiang, J. Mater. Chem. C **4**, 1704 (2016)
3. D. Jin, J. Yang, X. Miao, L. Wang, S. Guo, N. Wang, L. Wang, Mater. Lett. **79**, 225 (2012)
4. K.A. Koparkar, N.S. Bajaj, S.K. Omanwar, J. Rare Earths **33**, 486 (2015)
5. Y. Zhou, D. Chen, W. Tian, Z. Ji, J. Am. Ceram. Soc. **98**, 2445 (2015)
6. M. Takesue, H. Hayashi, R.L. Smith Jr, Prog. Cryst. Growth Charact. Mater. **55**, 98 (2009)
7. L. El Mir, A. Amlouk, C. Barthou, J. Phys. Chem. Solids **67**, 2395 (2006)
8. M. Mai, C. Feldmann, Solid State Sci. **11**, 528 (2009)
9. X. Li, F. Chen, Mater. Res. Bull. **48**, 2304 (2013)
10. D.T. Palumbo, J.J. Brown Jr, J. Electrochem. Soc. **117**, 1184 (1970)
11. L. El Mir, K. Omri, J. El Ghoul, Superlattices Microstruct. **85**, 180 (2015)
12. H. Hess, Phys. Status Solidi A **85**, 543 (1984)
13. Q.Y. Zhang, K. Pita, C.H. Kam, J. Phys. Chem. Solids **64**, 333 (2003)
14. N. Taghavinia, G. Lerondel, H. Makino, T. Yao, Thin Solid Films **503**, 190 (2006)
15. Y. Wu, Y. Wang, D. He, M. Fu, Z. Chen, Y. Li, J. Lumin. **130**, 1768 (2010)
16. N. Taghavinia, G. Lerondel, H. Makino, A. Parisini, A. Yamamoto, T. Yao, Y. Kawazoe, T. Goto, J. Lumin. **96**, 171 (2002)
17. Y.C. Kang, H.D. Park, Appl. Phys. A **77**, 529 (2003)
18. D. Chen, W. Xiang, X. Liang, J. Zhong, H. Yu, M. Ding, H. Lu, Z. Ji, J. Eur. Ceram. Soc. **35**, 859 (2015)
19. K. Omri, J. El Ghoul, O.M. Lemine, M. Bououdina, B. Zhang, L. El Mir, Superlattices Microstruct. **60**, 139 (2013)
20. J. El Ghoul, C. Barthou, L. El Mir, Phys. E **44**, 1910 (2012)
21. J. El Ghoul, C. Barthou, L. El Mir, Superlattices Microstruct. **51**, 942 (2012)
22. J. El Ghoul, C. Barthou, M. Saadoun, L. El Mir, J. Phys. B **405**, 597 (2010)
23. B.D. Cullity, *Elements of X-ray Diffractions* (Addison-Wesley, Reading, 1978), p. 102
24. S. Chakrabarti, D. Das, D. Ganguli, S. Chaudhuri, Thin Solid Films **441**, 228 (2003)
25. R. Selomulya, S. Ski, K. Pita, C.H. Kam, Q.Y. Zhang, S. Buddhudu, J. Mater. Sci. Eng. B **100**, 136 (2003)
26. N. Taghavinia, G. Lerondela, H. Makino, A. Yamamoto, T. Yao, Y. Kawazoe, T. Goto, J. Nanotechnol. **12**, 547 (2001)
27. A.L.N. Stevels, A.T. Vink, J. Lumin. **8**, 443 (1974)
28. S. Dembski, S. Ruppa, M. Milde, C. Gellermann, M. Dyrba, S. Schweizer, M. Batentschuk, A. Osvet, A. Winnacker, J. Opt. Mater. **33**, 1106 (2011)
29. J. Lin, D.U. Sanger, M. Mennig, K. Barner, Thin Solid Films **360**, 39 (2000)
30. A. Patra, G.A. Baker, S.N. Baker, J. Lumin. **111**, 105 (2005)
31. D.J. Robbins, N.S. Casewell, Ph Avouris, E.A. Giess, I.F. Chang, D.B. Dove, J. Electrochem. Soc. **132**, 2784 (1985)
32. C. Barthou, J. Benoit, P. Benalloul, A. Morell, J. Electrochem. Soc. **141**, 524 (1994)
33. L.E. Orgel, J. Chem. Phys. **23**, 1819 (1955)
34. L. Xiong, J. Shi, J. Gu, L. Li, W. Huang, J. Gao, M. Ruan, J. Phys. Chem. B **109**, 731 (2005)